CREATING AND EXPLICITLY CHARACTERIZING HETEROGENEITY AND NAPL MACRO-SCALE ENTRAPMENT AT THE INTERMEDIATE SCALE

Gilbert R. Barth[1,3], *Tissa H. Illangasekare*[2], *Harihar Rajaram*[1], and *Mary C. Hill*[3],
[1]Civil and Environmental Engineering, University of Colorado, Boulder, CO 80309-0428
[2]Env. Sciences and Eng., Colorado School of Mines, Golden, CO 80401-1887
[3]U.S. Geological Survey, 3215 Marine St., Boulder, CO 80303-1066

ABSTRACT

Two sequential, non-aqueous phase liquid (NAPL) injection experiments, performed in an intermediate-scale heterogeneous porous medium, provided the unique opportunity to explicitly characterize NAPL migration and high-saturation entrapment. A 10-meter long two-dimensional tank was filled with a heterogeneous packing using five different sands. The heterogeneity approximated a log normal distribution of hydraulic conductivity (K) with a mean ln$K$ value of 4.18 (m_{lnK}), where K has units of cm/hr, a variance of 1.22 (σ^2_{lnK} = 1.22) and an anisotropic exponential covariance structure. The horizontal (l_h) and vertical (l_v) correlation scales of ln$K$ were 50.8 and 5.08 cm, respectively, leading to an anisotropy ratio, l_v / l_h = 0.1. A light NAPL was injected into the bottom of the water-saturated heterogeneity. NAPL migration proceeded according to buoyancy and capillary forces, jumping vertically to coarse lenses and then following them laterally for large distances. Prior to entering any new cells, NAPL from the second spill resaturated cells traversed during the first spill and then infiltrated adjacent and nearby coarse cells. The rate of NAPL redistribution was monitored at several locations during infiltration, and its distribution mapped at quasi steady state, using a gamma system. Modified ln$K$ distributions were estimated using gamma-system-measured NAPL saturations and the Brooks-Corey relative-permeability function. Variograms of the modified ln$K$ distributions reflect the NAPL's tendency to occupy coarse sand regions, resulting in a large increase in σ^2_{lnK}. Variogram structure indicates that differences between the pre-spill and post-spill ln$K$ distribution occur at smaller separations: at separations greater than the spill extent, the post-spill variograms approach the pre-spill variogram. The results provide, (1) unique insight to the migration of NAPL in heterogeneous material, (2) demonstrate extreme contrasts in NAPL saturation and the influence of heterogeneity on NAPL distribution, and (3) provide considerable motivation for using integrated, as opposed to point, methods of NAPL spill characterization.

INTRODUCTION

The pervasive use of non-aqueous phase liquid (NAPL) has inevitably lead to a considerable number of sites contaminated by NAPLs. Unfortunately, there has been only limited work assessing the behavior of NAPLs for heterogeneous field sites[1] and laboratory experiments[2]. These investigations were forced to deal with different scales of heterogeneity and a more limited heterogeneous system, respectively. However, such work has illustrated the preference of NAPL for certain materials and the propensity for NAPL to be distributed almost exclusively in such materials, at high levels of saturation. This work presents a series of intermediate-scale laboratory experiments that recreate aspects of a field-site dense-NAPL (DNAPL) spill to examine the propensity for distribution and saturation under controlled conditions.

A 10-meter long two-dimensional tank was filled with a heterogeneous packing using five different sands, designed to represent a stationary ln$K$ field with anisotropic exponential covariance structure. NAPL was injected into the tank resulting in macroscale entrapment due to heterogeneity of the soil properties. A gamma system mapped the saturation distribution of NAPL in the tank. A second NAPL spill and subsequent gamma scanning provided additional insight to the entrapment and distribution of NAPL in the heterogeneous system.

INTERMEDIATE-SCALE EXPERIMENTAL SYSTEM

Heterogeneous Porous Media Construction and Instrumentation

The intermediate-scale porous medium was constructed in a tank approximately 10 meters long, 1.2 meters tall, and 0.06 meters inside width (Figure 1a). Each end of the porous medium consisted of a 20 cm section of pea gravel to provide constant-head boundaries for the system. The overall gradient and saturated zone thickness were adjusted with two constant-head tanks that controlled the water level in the pea gravel. The water table was level with the top of the sand packing at the up-gradient end of the tank. At the down-gradient end it was 15.7 cm below the top of the packing producing an overall gradient of approximately 0.016 along the length of the tank. Deionized water was supplied to the up-gradient constant-head tank. The gradient and resulting flow of approximately 3.2 L/hr were maintained throughout the experiments.

The packing within the tank consisted of two zones: a homogeneous section of coarse sand (#8 sieve) in the upstream 1.1 meters of the tank followed by an 8.1 meter heterogeneous section (Figure 1a). The heterogeneous zone served as a laboratory analogue of random field-site sedimentary structure, was created using five different sands, and designed to support explicit representation in a numerical model. The heterogeneous zone approximated a log normal distribution of hydraulic conductivity (K) with a mean ln$K$ value of 4.18 (m_{lnK}), where K has units of cm/hr, a variance of 1.22 (σ^2_{lnK} = 1.22) and an anisotropic exponential covariance structure. For comparison to well-known field sites, σ^2_{lnK} of the Cape Cod, Borden, and Columbus sites were 0.2[3], 0.24[4] and 4.5[5] respectively. The horizontal (l_h) and vertical (l_v) correlation scales of ln$K$ were 50.8 and 5.08 cm, respectively, leading to an anisotropy ratio, l_v / l_h = 0.1. At the Cape Cod, Borden and Columbus sites, l_v / l_h = 0.04, 0.02, and 0.01, respectively.

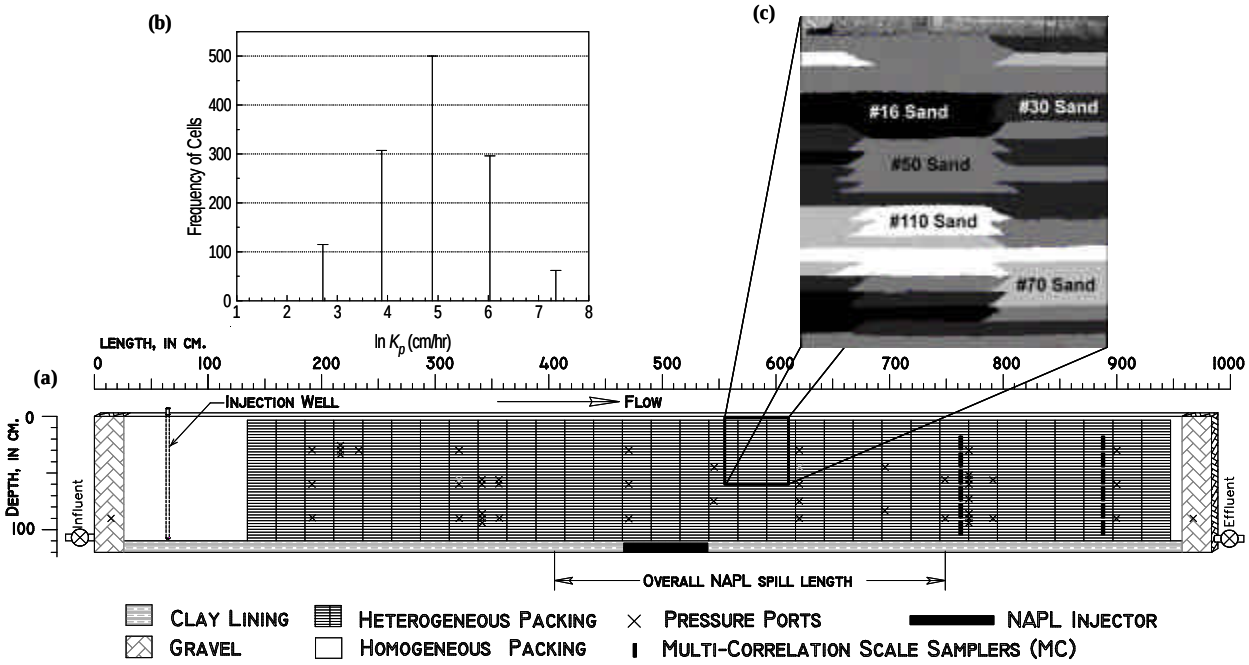

Figure 1: Intermediate-scale tank design showing (a) the dimensions of the entire tank including a simplified representation of the sand cell packing and the pressure and sampling ports, (b) the frequency distribution of sand cell packing for the five hydraulic conductivities (permeameter values are shown), and (c) an enhanced gray-scale detail of the tank packing. Each sand lens is 25.4-cm long and 2.54-cm tall, and is tapered at the ends as shown in (c).

Table 1: Sand Properties

	Mesh Size (ASTM E-11)				
	#16	#30	#50	#70	#110
K_p (cm/hr)	1550	417	133	48.6	15.1
d_{50} (mm)	0.88	0.49	0.30	0.19	0.103
d_{60}/d_{10}	1.72	1.50	1.94	1.86	NA
λ[1]	3.5	3.0	1.9	2.2	NA
S_r	0.07	0.26	0.28	0.30	0.30

[1] From Szlag, 1997

To design the heterogeneous packing, a continuous ln*K* distribution with the desired statistical structure was generated using a Fourier summation algorithm[6] and then discretized into five categories. Each category was assigned a particular sieve size sand: #16, #30, #50, #70 or #110 (Table 1). Values of m_{lnk}, s^2_{lnk} were evaluated and the match between correlation structure of the discretized distribution and the corresponding statistics of the original continuous distribution verified[7]. Measured hydraulic-conductivity values (K_p in Table 1) for each sieve size sand were determined by *Mapa et al*. [unpublished report for the U.S. Army Engineer Waterways Experiment Station, 1994]. The values of m_{lnK} and σ^2_{lnK} for the discretized distribution are as noted above. The frequency distribution of the five different sands in the heterogeneous packing is shown in Figure 1b. Simulated head and flow values did not match observations so nonlinear regression was performed to determine the optimal values of hydraulic conductivity, K_r[8], which provided the best fit between observations and predictions of heads and flows. The variograms of

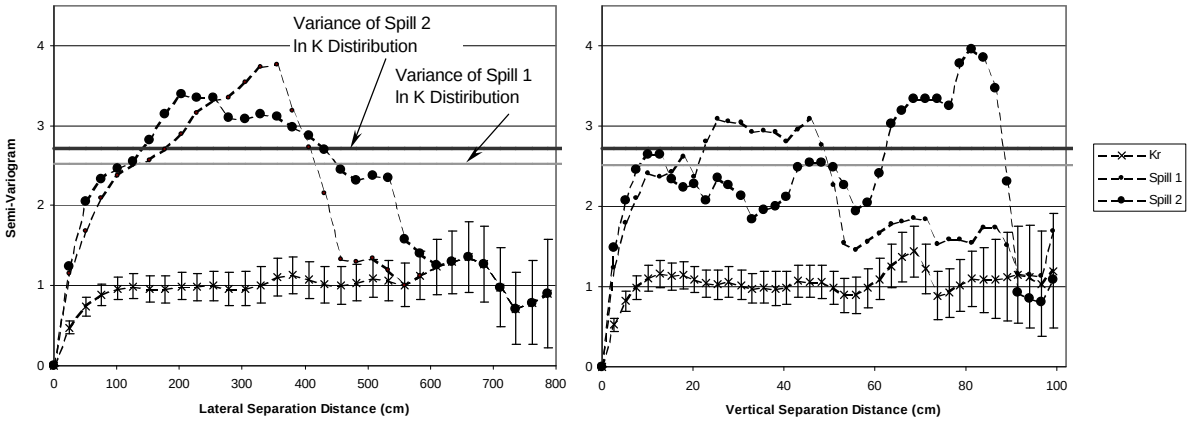

Figure 2: Variograms of the heterogeneous porous media. Each graph includes variograms based on: negative exponential covariance function using K_r values, with 95% confidence intervals indicated, and the distribution of effective permeability following the first and second NAPL spills. (a) Horizontal variograms. Structure from the 1st and 2nd spill persists for ~400 and 550-cm respectively. (b) Vertical variograms. Structure from the 2nd spill extends almost twice as far as the first spill. Large 1st spill increase in sill and minimal change for 2nd spill reflect the change in distribution variance with each spill.

lnK_r for the discretized distribution are shown in Figure 2 and match the targeted variograms corresponding to the exponential covariance function reasonably well.

NAPL-SPILL EXPERIMENTS

An aliphatic hydrocarbon, Soltrol 220 (Phillips Petroleum Company), was selected as the primary NAPL component for injection based on its relatively low toxicity. To represent a DNAPL sinking below the water table Soltrol, since it is lighter than water (r = 0.81 gm/cm^3), was injected from the bottom of the water-saturated heterogeneous packing. Soltrol was used because DNAPLs that are available for laboratory studies are typically more toxic and tend to corrode the walls of the Plexi-glass lined intermediate-scale tank. Soltrol was considered to be an experimental analog of fuel oil. The Soltrol was mixed with 1-Iodoheptane at a 1:9 ratio to produce a NAPL mixture with a gamma-particle attenuation coefficient of 0.72 cm^{-1}, significantly greater than water, 0.19 cm^{-1}, and density still significantly less than water, r = 0.83 gm/cm^3. Automate Red B (Morton International), a dark red organic dye essentially insoluble in water, was added to the Soltrol/1-Iodoheptane mixture at a ratio of 0.1% (volume/volume) to allow visualization of the spill. For the remainder of the paper the mixture of Soltrol 220, 1-Iodoheptane and Automate Red B is simply referred to as the NAPL.

The spill was created by injecting NAPL into the bottom of the heterogeneous formation. The injector consisted of a perforated PVC pipe wrapped with a stainless steel mesh and packed in #8 sieve size sand below columns 14, 15, and 16 of the heterogeneous packing (Figure 1a) producing a source of 1.5 l_h, or 76.2-cm long. The NAPL was injected at a rate of about 0.21 l/hr and 0.13 l/hour for the first and second spill, respectively. The length of injector and slow injection rate promoted lateral spreading of the NAPL[9] and preferential infiltration into coarser material[2] resulting in a spill distribution similar to that produced by a slow leak from a DNAPL tank (Figure 3). The first spill was 7.2 liters and an additional 4.2 liters were injected for the second spill. These spill volumes corresponded to 7 and 4 percent of the total pore volume in the tank.

Mapping the NAPL Distribution

This study evaluated a two-component system within the saturated zone: water and NAPL. A gamma ray attenuation system was used to measure NAPL saturations during and after the NAPL spills. The gamma system was used in two ways 1) immediately following each spill it monitored the rate of NAPL redistribution and 2) mapping of the NAPL saturation distribution after redistribution had reached a quasi-steady state. Detailed descriptions of the system have been published elsewhere[10,11]. As discussed below, the NAPL saturation data was used to calculate changes in local wetting-phase (water) permeability as a result of NAPL entrapment.

Characterization of the NAPL spills

Composited digital images of the first and second spill provide a qualitative indication of NAPL distribution for each spill and illustrate the dramatic contrasts in NAPL saturations and the complex pattern of spatial distribution (Figure 3). The images correspond to just over one-third of the entire tank length. Over a fourteen-day period the first NAPL spill spread approximately 50-cm in the vertical direction and 300-cm laterally. While these values summarize the extent of NAPL spreading they do not capture the highly discontinuous nature of the saturation distribution and the dramatic local contrasts in NAPL entrapment. The majority of redistribution occurred during the first 4 days (Figure 4). It should be noted that, following the first spill, the entire upper half of the tank remained free of NAPL. The first spill only reached coarse lenses in the bottom half of the tank. During the second spill all coarse lenses, from the top to the bottom of the tank, in the spill-impacted region were saturated with NAPL.

Photographic and gamma scan evidence suggest that NAPL from the second spill flowed through the same cells as in the first spill until most of the cells infiltrated during the first spill were fully re-saturated. After that, the NAPL began infiltrating new cells at the periphery of the first spill, moving preferentially into coarser material. NAPL migration jumped vertically to coarse lenses and then followed them laterally for large distances. In general, the additional cells infiltrated during the second spill were more widely dispersed than most of the cells infiltrated during the first spill. The first-spill region acted as a large injector, allowing the spill progress to selectively infiltrate into a sampling of cells more closely resembling the distribution as a whole. In addition, infiltration into new cells after the second spill occurred after injection pumping had ceased and was therefore a function of buoyancy and capillarity alone.

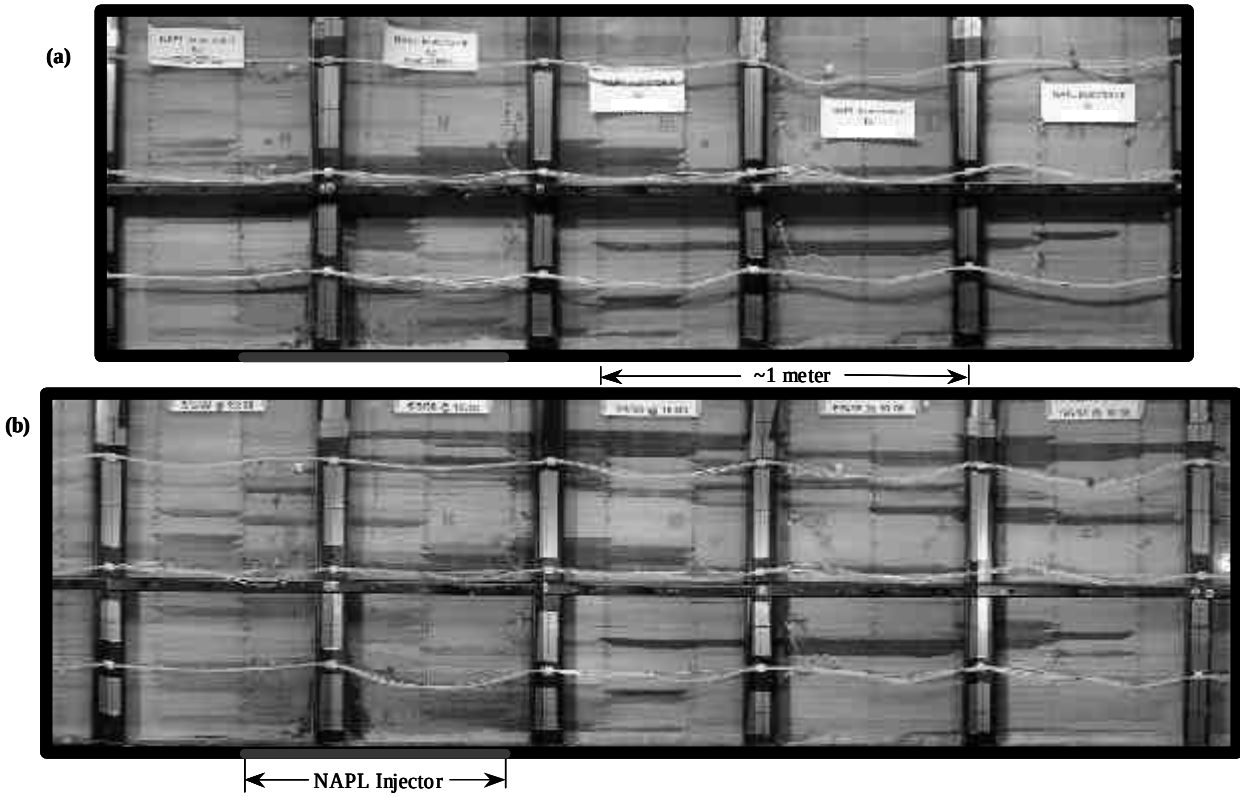

Figure 3: Composited digital images of NAPL entrapped in the intermediate-scale heterogeneous porous media. Images were taken after rapid redistribution had ceased. (a) After first spill of 7.2 liters. (b) After second spill of an additional 4.35 liters. Cluster of saturation above injector was an artifact of pumping NAPL. Distribution of cells infiltrated during 2nd spill provides a better indication of NAPL migration and distribution due to buoyancy and capillarity in this heterogeneous distribution of sands. The scales on the two images are approximately the same. The spill size and location are indicated in Figure 1a.

A notable feature of both spills is the apparently disconnected distribution of NAPL-saturated lenses. The absence of any visual or gamma-scan indication of NAPL in the finer lenses separating the NAPL-saturated coarse lenses suggests that pore-scale fingering was the primary means by which the NAPL moved between coarse lenses. Within coarse lenses, as saturation and the capillary pressure increased, NAPL penetrated the overlying finer lens only through the pores with the lowest pore-entry pressure. Initiation of NAPL fingers between non-adjacent coarse

lenses provided sufficient opportunity for the NAPL to progress between coarse lenses insuring that the capillary pressure never exceeded the average pore-entry pressure of the finer sands. As a result, NAPL transport and the resulting distribution shown in Figure 3 were determined by variability at the pore scale.

Figure 5 illustrates the NAPL's propensity to finger, selectively entering pores with the lowest pore-entry pressure. The image is from the vicinity of the NAPL injector. The combination of pumping, capillarity, and buoyancy forced NAPL into the #30 sand fully saturating it, was not sufficient to penetrate the #70 sand and only penetrated the #50 sand in portions that, as a result of packing-induced sorting, had slightly lower pore entry pressures. The same sensitivity to minor variations in pore size that produced this layered-saturation effect in a single lens led to the formation of discrete NAPL fingers connecting non-adjacent coarse lenses. The resulting discontinuous distribution of high-saturation lenses is illustrated in Figure 3. The packing-induced sorting illustrated in Figure 5 was atypical, only about one percent of all sand lenses demonstrated packing-induced sorting.

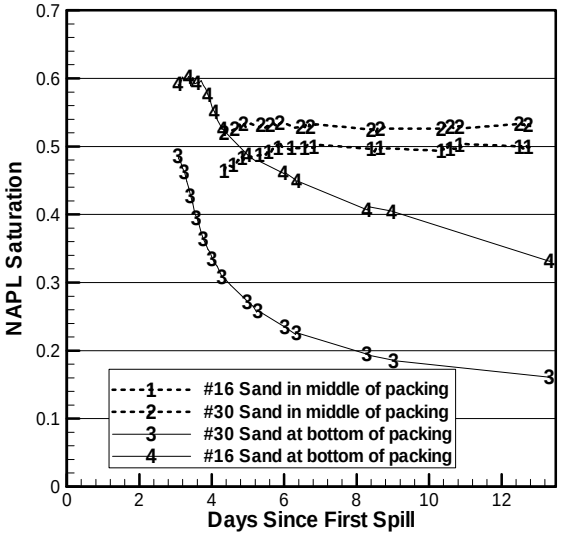

Figure 4: Change in NAPL saturation with time at four locations following the first spill. Lower cells drained as buoyancy drove the NAPL higher in the packing. Higher cells, at the upper extent of the first spill exhibited a relatively constant saturation during scanning.

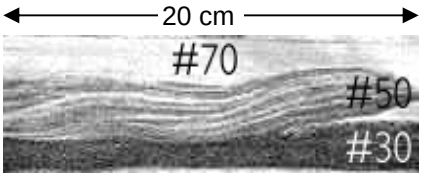

Figure 5: Discrete distribution of NAPL in #50 sand lens. NAPL fully saturated the lower pore-entry pressure #30 sand, could not infiltrate the finer #70 sand and selectively infiltrated the #50 sand in the regions where minor packing-induced sorting had resulted in slightly larger pore diameters.

Performing the same experiment or similar experiments using NAPLs of different density contrast, viscosity or surface tension would produce a similar discontinuous pattern of high-saturation lenses, connected by discrete fingers[2]. The spatial distribution would differ due to differences in the density contrast, viscosity or surface tension and the resulting differences in, (1) propensity to penetrate into finer or coarser material, (2) spread laterally and, (3) time required for rapid redistribution to cease. Use of dimensionless ratios such as the Bond number, Capillary Number would provide insight to the distribution of NAPLs with different physical properties, but was outside the scope of this work. Changes to the porous-media distribution would have a similar impact. For example, performing the same Soltrol NAPL injection in a heterogeneous packing with a different variance, correlation length, anisotropy or lens dimensions would result in a similar discontinuous pattern of high-saturation lenses connected by discrete fingers, but with a markedly different distribution of the NAPL.

The impacts of the NAPL spill on the hydraulic behavior of the medium can be quantified based on the modified wetting phase permeability resulting from NAPL entrapment. Although relative permeability was not measured directly, permeability modifications resulting from NAPL entrapment were estimated using the measured NAPL saturations and the Brooks-Corey relative permeability function:

$$k_{rw} = S_e^{(2+3l)/l} \qquad (1a)$$

$$S_e = \frac{S_w - S_r}{S_m - S_r} \qquad (1b)$$

where l is a pore size distribution index, S_e is the effective saturation and S_w, S_m and S_r are the wetting-phase, maximum, and residual saturation, respectively. For laboratory conditions, with relatively uniform media carefully saturated, the value of S_m is essentially equal to 1.0. The values of l and S_r corresponding to each sand were obtained from suction-saturation measurements[12] and are listed in Table 1. The modified ln$K$ distributions within the NAPL spill zone, reflecting the influence of NAPL entrapment are shown in the Figure 6. The frequency of large ln$K$ values is reduced in the modified distributions reflecting the tendency of the NAPL to occupy coarse sand regions. The spread of the distribution increases dramatically due to the very low hydraulic conductivity of the lenses with macroscale NAPL entrapment. The variograms of the modified ln$K$ distribution illustrate the change in spatial structure of the ln$K$ variation resulting from NAPL entrapment (Figure 2). The variogram sill reflects a dramatic increase in s^2_{lnK} after the first spill, and only a slight increase between the first and second spills. The shapes of the variograms also provide considerable insight to the spill distribution. In the case of the horizontal variogram, the major difference between the pre-spill and post-spill variograms occurs at smaller separations. At separations greater than the visually and gamma-scan determined extent of the spill, the post-spill variograms appear to approach the general trend of the pre-spill variogram. Agreement between the pre- and post-spill variograms at larger separations reflects the finite horizontal extent of the spill region. The range of separations over which the pre-spill horizontal variogram is modified increases after the second spill consistent with the increase in the horizontal extent of the spill. The vertical variograms exhibit a similar response for the first spill. The vertical extent of NAPL following the 2nd spill results in vertical variograms that do not match the pre-spill variograms over the entire range of separations (Figure 2).

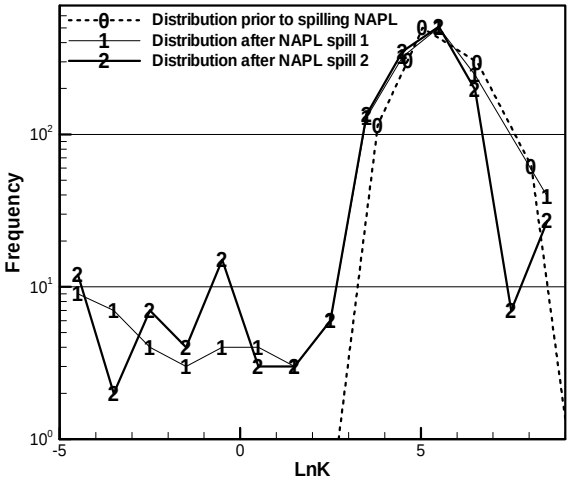

Figure 6 Distribution of ln$K$ initially, (0) and following NAPL spill one, (1) and two, (2).

DISCUSSION/CONCLUSIONS

Five different sands with hydraulic conductivities spanning more than two orders of magnitude (m_{lnK}= 4.18, σ^2_{lnK} = 1.22) were used to create an anisotropic heterogeneous porous medium in a 10m x 1.2 m intermediate-scale experimental tank. The contrasts in porous medium material properties provided the opportunity for high-saturation NAPL entrapment. Two injections of a light NAPL, into the bottom of the saturated porous medium, created a spill analogous to a DNAPL penetrating below the water table and redistributing as a function of

buoyancy and capillarity. Visual inspection and scanning with a gamma system revealed, (1) the discontinuous nature of the NAPL distribution as a function of the porous medium heterogeneity, and (2) the propensity for high saturation entrapment.

Although the experimental studies presented here were carried out in a two-dimensional system, similar behavior is plausible in three-dimensional field systems. For instance, the most important feature of the entrapped NAPL distribution, i.e., macroscale entrapment within coarse lenses, has been observed in the field[1]. For large spill volumes in field settings, macroscale entrapment can be expected. For example, using the Borden site parameters, if we consider the dimensions of a typical coarse lens to be of the order of a correlation length in each direction, the pore volume inside such a lens is only about 0.75 m^3. Thus, a large spill can readily lead to macroscale entrapment and local NAPL saturations that are much larger than residual.

This study produced quantitative estimates of the NAPL saturation distribution in an intermediate-scale heterogeneous porous medium. A review of the literature did not reveal any previous experiments involving NAPL spills in a realization of a random field at the scale of the experiments presented, with fine-scale resolution of the heterogeneity. The experimental data on NAPL saturations are potentially useful for evaluating models of NAPL migration in heterogeneous porous media. In particular, it appears that models based on the continuum multiphase flow equations are not capable of predicting the pore-scale fingering which seems to have produced the discontinuous distribution of NAPL saturation. However, recently developed models based on percolation theory[13,14] appear promising. The dataset produced should serve as a useful, high-quality dataset for testing and improving models of NAPL migration.

REFERENCES

[1]Kueper, B. H., D. Redman, R. Starr, S. Reitsma, M. Mah, Ground Water, 31(5):756-766, 1993.
[2]Compos, R., M. S. Thesis, University of Colorado, 126 p., 1998.
[3]Hess, K. M., S . H. Wolf, and M. A. Celia, *Water Resour. Res.*, 28(8):2011-2027,1992.
[4]Woodbury, A. D., and E. A. Sudicky, *Water Resour. Res.*, 27(4):533-546, 1991.
[5]Boggs, J. M., S. C. Young, D. J. Benton and Y. C. Chung, EPRI EN-6915, July, 1990.
[6]Shinozuka, M. and C.-M. Jan, *J. of Sound and Vibration*, 25(1):111-128, 1972.
[7]Chao, H-C, H Rajaram and T H Illangasekare, Ann. Fall AGU Meeting, 1996.
[8]Barth, G. R., M. C. Hill, T. H. Illangasekare and H. Rajaram, *Water Resour. Res*, in press, 2001.
[9]Kueper, B. H. and J. I. Gerhard, *Water Resour. Res.*, 31(12), 2971-2980, 1995.
[10]Illangasekare, T. H., D. Znidarcic, G. Walser and J. Weaver, EPA/600/R-94/197, 1994.
[11]Walser, G. S., Ph. D. Dissertation, University of Colorado at Boulder, 255p., 1995.
[12]Szlag, D., Ph.D. Dissertation, University of Colorado, 1997.
[13]Ewing, R. P., and B. Berkowitz, *Water Resour. Res.*, 34(4):611-622, 1998.
[14]Glass, R. J., S. H. Conrad, and L. Yarrington, *Water Resour. Res.*, 37(5):1197-1207, 2001.